OPEN ACCESS

1st International e-Conference on Energies
14 - 31 March 2014

http://sciforum.net/conference/ece-1

Conference Proceedings Paper - Energies "Whither Energy Conversion? Present Trends, Current Problems and Realistic Future Solutions"

Negative Triangularity Tokamak as Fusion Energy System

M. Kikuchi[1], A. Fasoli[2], T. Takizuka[3], P. Diamond[4], S. Medvedev[5], X. Duan[6], H. Zushi[7], M. Furukawa[8], Y. Kishimoto[9], Y. Wu[10], O. Sauter[2], L. Villard[2], S. Brunner[2], G. Merlo[2], J.M. Kwon[4], G. Zheng[6], K. Mishra[7], M. Honda[1], H. Urano[1], M.J. Pueschel[11], D. Told[12], A. Fujisawa[7], K. Nagasaki[9], F. Sano[9]

[1]Japan Atomic Energy Agency, Japan , [2]CRPP-EPFL, Switzerland , [3]Osaka University, Japan , [4]World Class Institute, NFRI, Korea , [5]Keldysh Institute of Applied Mathematics, Russia , [6]Southwestern Institute of Physics, China , [7]Kyushu University, Japan , [8]Tottori University, Japan , [9]Kyoto University, Japan , [10]Institute of Nuclear Energy Safety Technology, CAS,China , [11]University of Wisconsin-Madison, USA , [12]Max Planck Institute fur Plasma Physics, Germany

* Author to whom correspondence should be addressed; kikuchi.mitsuru@jaea.go.jp

Received: 15 January 2014 / Accepted: 13 March 2014 / Published: 14 March 2014

Abstract: Fusion energy development is quite successful in both getting equivalent energy break-even condition in large tokamak and clarifying many important physics in the magnetically confined plasma to proceed to a fusion experimental reactor, ITER [12]. Now, fusion research has to solve the power handling toward fusion demonstration power reactor (DEMO). A tokamak plasma with strongly negative triangularity may offer such an opportunity as an innovative concept [2]. Experimental and theoretical works at CRPP-EPFL shows promising results for negative triangularity tokamak [31]. In this paper, we review the current understanding of such configuration in both physical and technological aspects.

Keywords: Fusion energy, Power handling, Tokamak, Negative Triangularity

---

1. Introduction

Tokamak is a frontrunner in fusion research with its excellent plasma confinement capability [12]. While the present tokamak system is operating in pulse, it has promising opportunity to become a continuous fusion power system if an intriguing physical phenomena, called bootstrap current is effectively utilized [8]. Tokamak configuration is optimized to have the best core plasma confinement leading to D-shaped plasma, which has a high edge pressure limit and is consistent with the reduced edge

transport by the H-mode operation. Lots of work have been done for this configuration to find promising solution for power and particle control.

In this paper, we give a global view of the key issue and ways to find promising solution of the power and particle control of tokamak fusion power station. Section 2 gives a comparison of fusion power handling with other energy systems. Section 3 gives an introduction to the power handling in tokamak and summary of recent findings of physics behind the power handling.

2. Power-handling Challenge in Fusion

2.1. Transient and Steady-state Heat Loads in Fusion

Any energy system has an interface between the heat source and coolants. In the fossil plants, the heat source is the chemical energy of the fuel burn and coolants are water or gas. In the light water fission reactor (LWR) plants, the heat source is the nuclear energy of the fuel fission and the coolant is the water.

Heat flux is a key parameter and Fig.1 shows (heat flux, duration) diagram for fossil, fission and present fusion design. Existing power system such as fossil and LWR produce electrical power continuously under the maximum heat flux of $0.3MW/m^2$ for fossil power plant and $1MW/m^2$ for the LWR. In case of fossil power plant, burning coal, oil and natural gas is relatively easy but the maximum heat flux is kept low to ensure high reliability and also high temperature operation using the high temperature gas cooling even with lower heat extraction capability of the gas. In case of LWR, fuel rods are distributed volumetrically and the total surface area is in proportion to the volume giving surface to volume ratio quite high.

Figure 1. Heat flux as a function of duration in Fossil power plant, Light Water Reactor, and Fusion System. Fusion system has two types of heat loads, in steady and in transient. For comparison, radiation heat flux at the surface of the Sun is also shown. Geometries of heat exhaust in Fossil, LWR and Fusion power are shown as well.

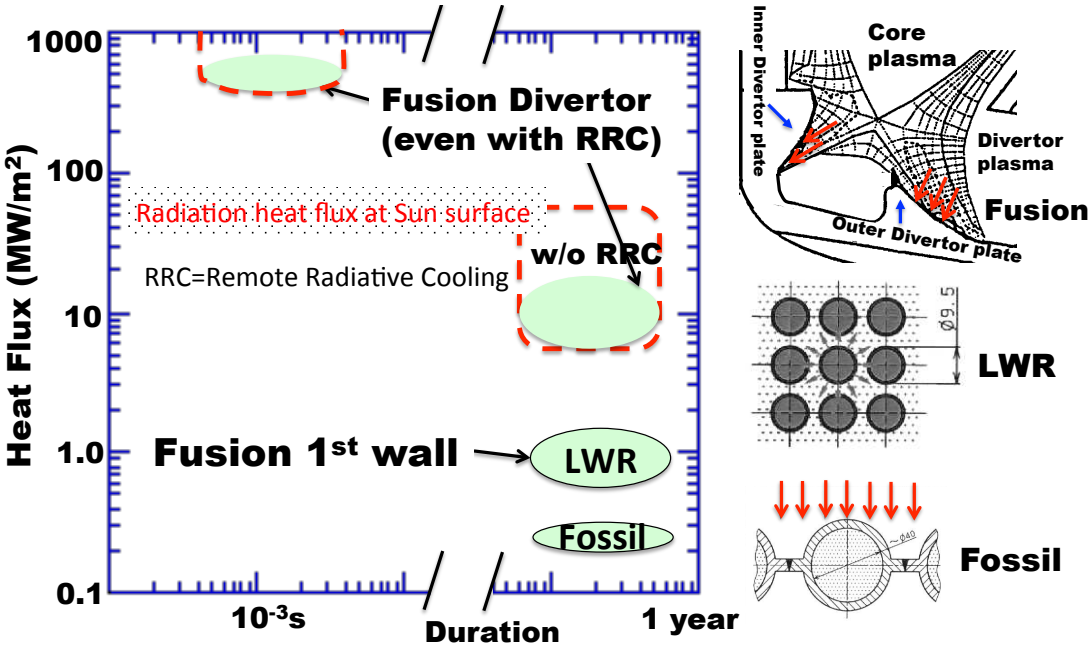

In the case of fusion, we have two types of heat fluxes, namely the steady state heat flux $\sim 10-20MW/m^2$ and also the transient heat flux $1-7MJ/m^2/ELM$ assuming heat exhaust area of $3m^2$ for the ELM. Here ELM is the abrupt energy release process triggered by the MHD instability, called the 'Edge Localized Mode'. Since most likely ELM energy loss is $7MJ/m^2$ in ITER, the suppression of this ELM energy loss is now one of major research elements in the world tokamak program targeting to reduce to $0.5MW/J$. Order of magnitude reduction in ELM energy loss is a big challenge but it is still for $\sim$ 300 full power discharges in ITER [3]. Suppression methods include the application of non-axisymmetric magnetic field called Resonant Magnetic Perturbation (RMP) [32] to make the edge magnetic fields partially ergodic and/or the high repetition injection of the hydrogen ice pellet [37] for pace making of transient energy loss from the edge plasma.

2.2. Divertor Concept in Tokamak

Fusion research is focused on D-T fusion reaction, where only 20% of the fusion power comes as 'HEAT', while 80% is carried by the 14MeV neutrons. Neutrons has large stopping range and the energy can be deposited volumetrically. Therefore D-T fusion should be much easier on the power handling than non neutron producing fusion reaction such as $D-He^3$ reaction.

Figure 2. a) Tokamak flux surface and the Divertor Geometry. b) SOL/divertor density contour plot for SSTR (attached divertor) [54]. The particle flux across the separatrix is $\Gamma_p = 2.5\times10^{23}/s$ assuming $\tau_p = 0.5s$, while $\tau_E = 1.4$. Bohm diffusion $D = D_B$ and $\chi_e = \chi_i = 2D_B$ are assumed for the SOL transport coefficients. To achieve dense and cold divertor plasma, intensive deuterium and impurity gas puffs are necessary near the inboard divertor $(\Gamma_{in} = 3\Gamma_p, \Gamma_{imp} = 0.015\Gamma_p)$ and the outboard divertor $(\Gamma_{out} = 4\Gamma_p, \Gamma_{imp} = 0.01\Gamma_p)$. c) Variation of the electron temperature (T_e) and the electron density (n_e) closest to the separatrix along the poloidal length from outer divertor plate to inner divertor plate. SOL pressure of DEMO is typically ~ 0.1 atm.

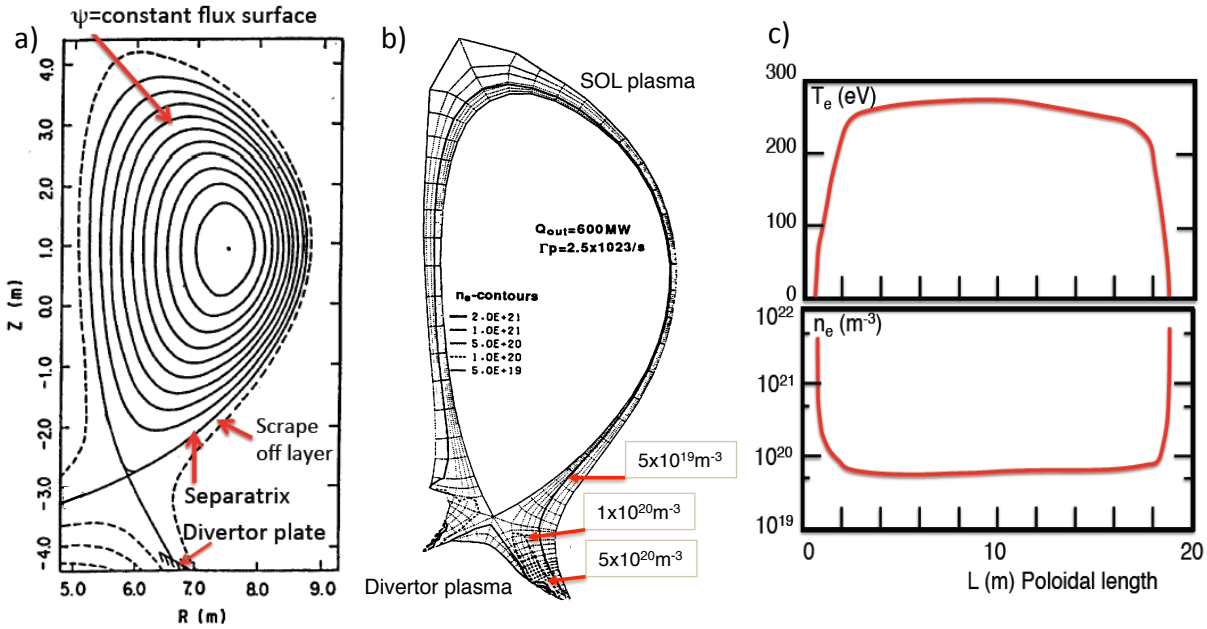

Let us think a case of SSTR [56] as a typical example of the tokamak fusion reactor. The surface area of the first wall is $700m^2$ in SSTR for the fusion power of $3GW$ of which $600MW$ is α heating power and the external heating and current drive power of $60MW$. Simple calculation is,

$$q_{heat} = \frac{660MW}{700m^2} = 0.94MW/m^2 \tag{1}$$

This level of heat flux should be able to exhausted by an existing heat engineering technology. But the situation is not so simple because of the localization of the heat.

The heat flux across the separatrix follows the open field line to the diverter plate and the effective width for the peak heat flux is relatively narrow of the order of $\sim 1cm$ even for the L-mode. The target heat flux width may be limited to 10cm the even if we have a flux expansion from the mid plane to the divertor plate ($\times 3$) and target inclination $1/sin\theta \sim 3.3$. The heat flux becomes very high if there is no radiative cooling.

$$q_{heat} = \frac{660MW}{2\pi \times 7m \times (2 \times 0.1m)} = 75MW/m^2 \tag{2}$$

This level of heat flux is comparable to the radiation heat flux of the Sun at its surface. The surface temperature of the Sun is $T_{eff} \sim 5778 \pm 3K$. Using the Stephan-Boltzmann law $q = \sigma T^4$ where $\sigma = 5.67 \times 10^{-8} W/m^2/K^4$, we have radiation heat flux at the surface of the Sun as $q_{Sun} = 5.67 \times 10^{-8} W/m^2/K^4 \times (5778K)^4 = 63MW/m^2$.

Tokamak reactor configuration equips with the nested flux surface in which high temperature core plasma ($T > 20keV, n_e > 10^{20} m^{-3}$) is confined and the outermost closed flux surface is called the separatrix having X point. The outside of the separatrix called SOL (Scrape-Off Layer) is not closed having open field line to the divertor plate as shown in Fig 2 a) to separate the high temperature plasma from the wall, which is sometimes called the magnetic limiter. This diverter concept is also effective to reduce the impurity influx to the high temperature core plasma originated from the divertor plate.

While high temperature core plasma is separated from the material surface, there exists high density plasma in the SOL and near the divertor plate. Fig2 b) shows a typical calculation for attached plasma for SSTR (Note that outer divertor target geometry is not good for particle compression and Slim-CS divertor [6] is better). The density near the divertor plate is much higher than that in the plasma center ($n_{div} \sim 10^{22} m^{-3}$) as seen in Fig.2 c). Actually, recent design of Slim-CS divertor [6] shows that the plasma density near the target plate is $n_{div} \sim 10^{22} m^{-3}$ to achieve nearly detached plasma. All these divertor plasma control needs sophisticated fuel and impurity gas puffing simultaneously to reduce heat flux $q_{div} \sim 10MW/m^2$ and plasma ion and electron temperatures under the steady state condition. The stability of the detached plasma is of significant importance.

The electron energy balance in SOL is governed by the balance between the perpendicular thermal conduction and the parallel Spitzer conduction. In principle, it is possible to reduce SOL T_e through impurity radiation control. Ion temperature in SOL, however, is higher than the electron temperature and not possible to reduce through radiation. Thus the ion heat flow can make a significant contribution to the heat flux to the divertor.

The previous assessment of the power handling in ITER [27] estimates the power e-folding length λ_q at the outboard mid-plane scrape-off layer (Fig.3 a)) as $\lambda_q = 5mm$. Recent paper by Goldston [9]

showed a model of the power e-folding length in the scrape-off layer (SOL) $\lambda_q \sim 2(a_p/R_p)\rho_{pi}$ and has no size dependence, where ρ_{pi} is the poloidal ion gyro radius. It predicts $\lambda_q = 1 - 2mm$ for the ITER. This scaling has been confirmed experimentally [14]. There are two key physics for such a narrow heat channel width, one of which is the reduced particle flux in the H-mode to the neoclassical drift flux [9] and the other is a very strong parallel flow speed $u_{\|} \sim 0.5C_s$, where C_s is a sound speed.

Figure 3. a) ITER divertor configuration and SOL flux lines [42]. b) Tokamak geometry with neoclassical toroidal drift speed v_d and the return parallel flow $u_{\|}$ in the SOL [9].

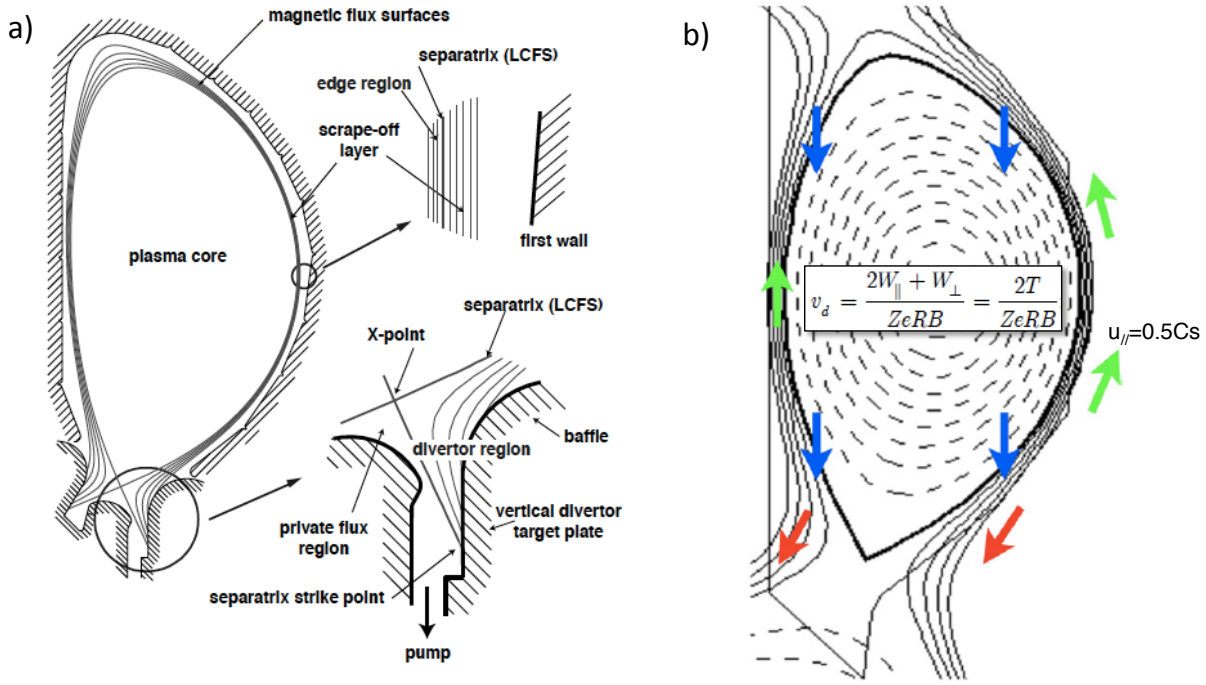

2.3. Narrow Heat Channel in the H-mode SOL

The SOL-divertor simulation for the fusion reactor has been done using the SOL fluid model [55]. The SOL fluid model do not reproduce experimentally measured large SOL flow speed ($u_{\|} \sim 0.5C_s$), which is thought to be a mystery until quite recently[30].

Takizuka [21], [15] showed by the particle simulation that the parallel convective heat flux could be enhanced by the SOL flow acceleration due to the ion orbit excursion across the separatrix up to $u_{\|} \sim 0.5C_s$. Fig.4 a) shows a schematic view of the flow pattern in tokamak in the case of ion ∇B drift away from the X point. Due to conservation of canonical angular momentum, both the trapped and the passing ions have radial excursion. Both co-passing and trapped ions cross the separatrix from the core at the low field side (larger R), have a velocity co to the plasma current, i.e. $u_{\|i} > 0$. These ions kick the SOL ions to have high flow speed parallel to the plasma current. On the other hand, the drift orbit of the counter passing ions shifts to the high field side and the counter passing ions kick the SOL ions to the counter direction (to the plasma current) to the order of $0.5C_s$. Such behavior is confirmed in the PARASOL simulation (Fig.4 b)).

The SOL-divertor fluid modeling has to include finite orbiting effect as well as transport coefficients valid for collision less regime not based on Braginskii fluid mode such as thermal force.

Figure 4. a) Schematic view of the particle drift orbit shapes, ∇B drift (red arrow) and the SOL return flow (green arrow). b) Particle simulation of SOL flow in a tokamak by PARASOL code [15]. Both for a case of ion ∇B drift away from X point.

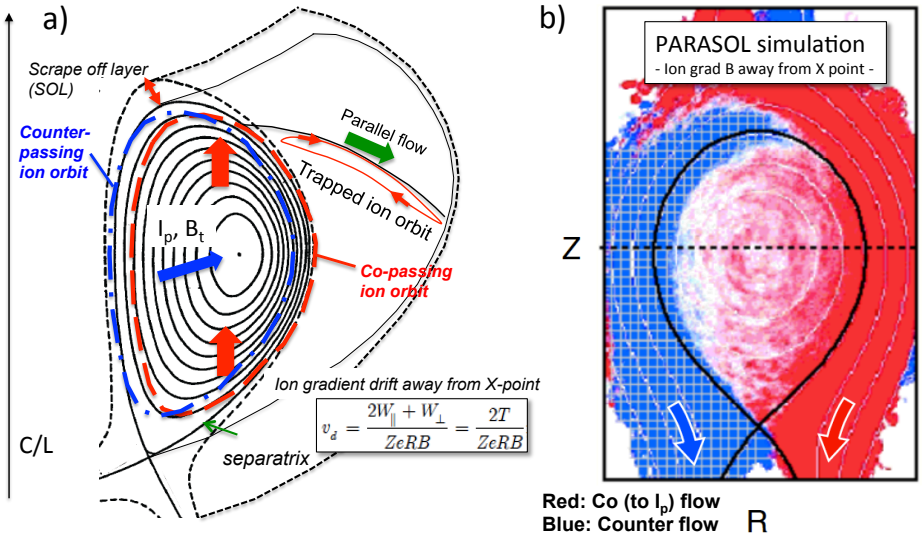

In good H-mode, it is shown that the particle flux across the separatrix is close to the neoclassical drift flux [9]. While the ion vertical drift motion supplies particles to the SOL across the separatrix, they are transfer back to the bottom by the parallel flow along the B field line in the SOL. While the ion parallel heat flow is dominated by the ion convection, the electron parallel heat flow might be dominated by the Spitzer heat conduction. Since $T_i > T_e$ in the SOL, heat flux is dominated by the ion convective flux. Ion continuity equation can be given by $l_\parallel \langle V_d \rangle = \lambda_q u_\parallel$. Using $l_\parallel = Rq$, $\langle V_d \rangle = 2T/ZeRB$, and $u_\parallel = 0.5C_s$, we have $\lambda_q \sim (a/R)\rho_{pi}$, where ρ_{pi} is ion polodal gyro-radius [9]. This scaling has been confirmed experimentally [14] predicting $\lambda_q^{ITER} \sim 1$ mm.

These modeling and experimental researches showed that the heat flux mitigation is a critical issue more than expected before.

2.4. ELM Heat load by High Edge Pedestal

Another key element in tokamak power handling is the transient heat flux due to ELM (type I ELM) as discussed in section 2. Fig 5 a) shows how such a transient heat flux come from the main plasma. This ELM energy loss ΔW_{ELM} over the pedestal plasma stored energy (energy between green and red line in Fig5 b)) depends on the edge collisionality ν^* as given by Loarte in 2003 [38]. If $\Delta W_{ELM}/W_{ped} = 0.2$ happens for the ITER, $\Delta W_{ELM} \sim 21MJ$ is expected for $W_{ped} = 0.3W_{th}$, $W_{th} = 350MJ$ in ITER. The effect of this ELM energy loss can be imagined since this energy loss is comparable to the total plasma energy of large tokamaks[33]. For a ELM interaction surface area $3m^2$, ITER ELM energy density is $\sim 7MJ/m^2$. Such a high transient energy deposition is quite damaging for divertor plate and reduction of ELM energy loss to $\sim 0.5MJ/m^2$ is envisaged to reach ~ 300 full power discharges having $\sim 10^5$ ELMs within a divertor lifetime [3]. This requires 14 times reduction.

Assuming ELM frequency $\sim$ $1Hz$, DEMO operating for 300 days has $25,920,000$ ELMs. Development of DEMO relevant ELM mitigation techniques is still a horizon after the ITER success.

The increase of ELM energy loss at low collisionality is attributed to the increase of the edge bootstrap current illustrated in Fig5 c). The increase of the surface current (i.e. edge bootstrap current) destabilize lower n (toroidal mode number) peeling eigenmode, which has larger radial extent [22]. Mitigation of ELM strength becomes essential for ITER and especially for future DEMO reactor, which necessarily operates high duty factor to effectively breed tritium.

As possible countermeasures to mitigate ELM strength, both Resonant Magnetic Perturbation (RMP) [32] and the pellet pace making [37] are actively pursued and are successful. However, application of RMP to divertor tokamak produces new magnetic field structure called "lobe" near the separatrix [23],[18], well-known in Dynamical System as "Homoclinic Tangle" originating from H. Poincare. This gives rise to an enhanced non-axisymmetric field perturbation near the X-point. These may be temporary measures for ITER but applicability to DEMO and beyond is still an open question.

We have some softer ELM activities such as type-III ELM [51], grassy ELM [45], type-II ELM [44], QH-mode [43]. Hastie [39] developed non-ideal effect not only ω_* effect but also ion sound wave and is used to explain small ELM in JT-60U [10]. If we want to keep our plasma to exhibit small ELM, we have to design the plasma shaping to keep high n ballooning mode as most unstable mode. Once we stabilize high n ballooning mode by entering the second stability, we can expect high β_N but also inevitably have type-I ELM, i.e., low n peeling-ballooning modes.

Figure 5. a) Schematic diagram of ELM energy loss. High edge beta limit in D-shaped plasma and edge transport barrier formation by the H mode give rise to the much higher plasma pressure than the L mode. High pedestal pressure gradient destabilize MHD instability and large loss of the plasma energy shown by the black arrow. b) $\Delta W_{ELM}/W_{ped}$ as a function of edge collisionality summarized by Loarte [38]. As edge collisionality reduces, $\Delta W_{ELM}/W_{ped}$ becomes large and $\Delta W_{ELM}/W_{ped} \sim 0.2$ may be possible at ITER collisionality. c) H-mode has steep pressure gradient near the edge and the edge bootstrap current increases with reduced edge collisionality. This surface current excites lower n peeling modes having wider radial mode width.

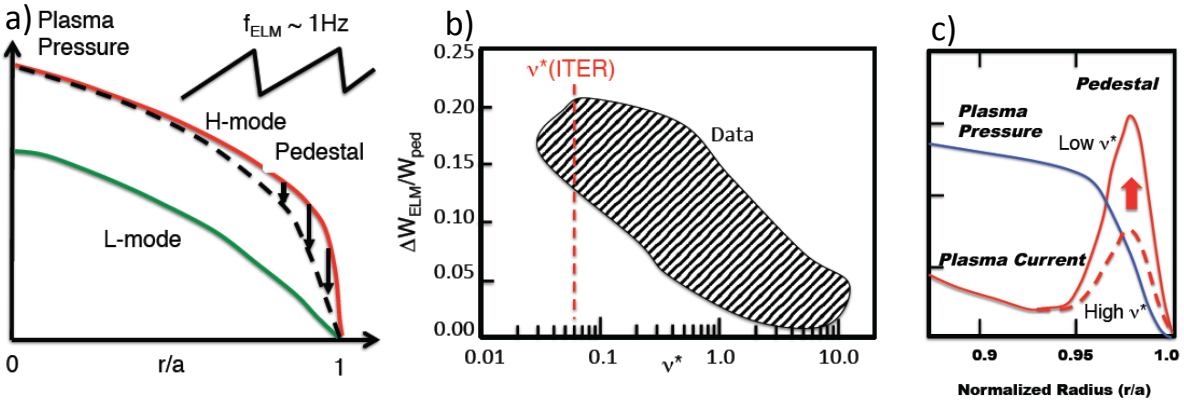

3. Lessons for Fusion Reactor Design Philosophy

We can identify many key questions and elements for fusion reactor design philosophy from our experiences described above.

3.1 Particle out flux : If we use Goldston scaling of H-mode particle flux $\Gamma_H = 4\pi a n_{sep} T_{sep}/B$, we have $\Gamma_H = 2.8 \times 10^{22}/s$ for $a = 1.7m, n_{sep} = 7 \times 10^{19}/m^3, T_{sep} = 300eV, B = 7T$. This is order of magnitude smaller than the assumed value for SSTR. While ELM provides large particle out flux to compensate this drawback, next generation ELM is now too strong.

3.2 High edge pedestal : High edge pedestal is achieved through strong shaping (high elongation κ and high triangularity δ). These shaping leads to the stabilization of the high n ballooning modes through access to the second stability regime and the most unstable mode becomes low n peeling/ballooning modes, which is the main cause of type-I ELM energy loss. For the reliable reactor operation, so-called soft-beta limit is highly desirable. Can we realize plasma configuration having such a soft beta limit with acceptable beta limit.

These two questions leads to a fundamental question to our choice of the confinement geometry:

Is D-shaped H-mode optimum choice? : Strongly D-shaped H-mode plasma is our choice for ITER and beyond. D-shaped configuration gives $R_{div} \ll R_p$, which makes power handling more challenging. Is D-shaped H-mode choice optimum for fusion power system, if the power handling is so important to solve? Radical question may be "Shall we stay at L-mode edge?" or "Shall we kill H-mode and seek for different improved confinement mechanism?".

General question to the design philosophy of tokamak fusion system is :

Core the first or power handling first? : Theory and experiments in tokamak research made a significant progress in understanding and confirming superiority of D-shaped H-mode scenario as a promising scenario to reach technical mission for ITER. But this configuration is optimization for the core confinement but has many drawbacks for the power handling, namely core the first design choice for the fusion power system. If we understand power handling is so critical for the success of fusion energy, shall we take a design philosophy of power handling the first?

Another interesting physics question is :

3.3 Fast SOL flow : Narrow heat channel width comes from fast SOL flow $u_{\|} \sim 0.5 c_s$ implied from new Goldston scaling. Is this coming from neoclassical orbiting effect? If so, can we find any confinement geometry which can reduce this SOL flow.

Above questions may ask us to explore wider design approach to fusion system based on power handling the first for the tokamak configuration design in addition to the standard D-shaped H-mode scenario. We illustrate negative triangularity-shaped tokamak as an example for such a design.

4. The Negative Triangularity-shaped Tokamak

To reconcile a challenging situation given in section 2, we may need larger reduction in the heat flux compared with the standard D shaped X-point divertor tokamak. We propose a tokamak configuration with a strongly negative triangularity as a possible operating scenario [2].

Standard tokamak reactor design such as SSTR [56] utilizes above mentioned ' core-the-first ' design philosophy, which leads to an excessive heat flux without any control of heat flux to $\sim 70MW/m^2$ close to the radiation heat flux at the surface of the Sun. Even if we use a sophisticated radiative cooling scheme in the core and the edge, we have typical heat flux $\sim 10MW/m^2$ [55]. Since the maximum heat fluxes for conventional power plants are $\sim 0.3MW/m^2$ for the fired plant and $\sim 1MW/m^2$ for the fission plant, such high steady state heat flux casts a question of the operational reliability of the fusion power station even if a plasma facing component to withstand such a high heat flux is developed. While we have made significant effort to realize such a divertor control during last two decades, we still do not have a good success with standard ' core-the-first design '.

The use of snowflake (SF-divertor) is proposed to expand the heat flux width larger than standard D shaped tokamak by a factor of $F = 1.5 - 3$ by Ryutov [29],[24] but this configuration requires too much PF coil currents for the standard D shaped tokamak reactor. Recent studies by Asakura [7] shows that internal poloidal field coils are necessary to realize the snowflake configuration and the required Ampere turn is $> 100MAT$ for a plasma current of $16.7MA$.

The strongly D shaped plasma leads to the divertor position to have smaller major radius than the plasma major radius, $R_{div} < R_p$, and the heat flux at the divertor plates is apt to enlarge. Accordingly, some countermeasures to reduce the transient and steady divertor heat loads in a tokamak reactor should be adopted such as the resonant magnetic perturbation (RMP) [32] and the pellet pace-making [37] for the ELM and the enhanced radiative-cooling in the core and the edge plasmas.

Configuration: Let us consider three geometries shown in Fig. 6 with a positive triangularity ($\delta = 0.8$) single null (SN) (Fig.2a)) and a negative triangularity ($\delta = -0.8$) SN with SF-divertor(Fig.2b)) and a negative triangularity ($\delta = -0.9$) double null (DN) (Fig.2c)). We consider a typical example at $R_p = 7m$, $A = R_p/a_p = 2.6$. With positive triangularity, we have $R_{div}^{\delta>0} = 4.0m$. On the other hand, we have $R_{div}^{\delta<0} = 10.0m$.

Since the power handling area for the divertor $S_{div} \sim 2\pi R_{div}(F\Delta)$, where Δ is effective width of the heat flux at the divertor plate for a standard X-point configuration including effect of inclination of the divertor target. F is the enhancement factor due to the SF flux expansion. Since $R_{div}^{\delta<0}/R_{div}^{\delta>0} = 2.5$ and $F = 1.5 - 3$ is expected [24], negative triangularity SF-divertor tokamak may have effective area enhancement $4 - 7$ over the standard D-shaped tokamak. If such an enhancement factor is realized, the solution to the power handling in the tokamak reactor may be technically more feasible by changing the uncontrolled heat flux from $70MW/m^2$ to $\sim 10MW/m^2$. To achieve uncontrolled heat flux $q_{div} \sim 10MW$ at $R_{div} = 10m$, we have to have heat flux width $F\Delta \sim 0.5m$.

Negative triangularity DN may also have such an enhancement factor but has issues related to the axisymmetric instability and the reduction of the tritium breeding ratio (TBR) due to the reduction of the coverage of the blanket, while there are some merits for Fig6 c).

Figure 6. Equilibrium configurations and SOL flow patterns for a) Standard D shaped Tokamak, b) Negative triangularity SF-divertor Tokamak, and c) Negative triangularity DN Tokamak (∇B drift away from X-point for SN cases).

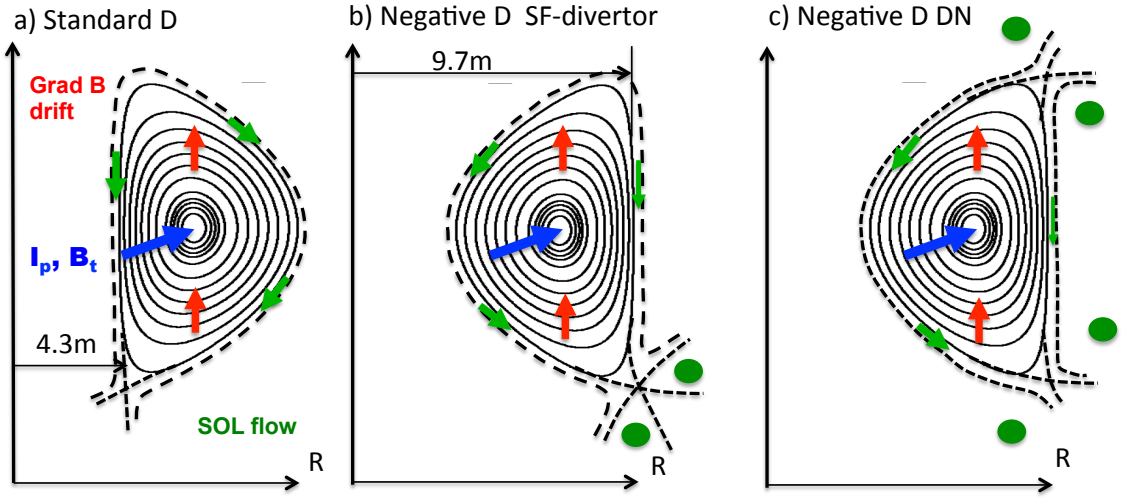

SOL flow physics of Negative Triangularity:

While we expect strong SOL flow in the standard D-shaped plasma, the SOL flow patterns may be different among 3 cases in Fig.6. In case of Fig 6 b) and c), SOL flow acceleration in the inboard side due to the counter passing ions is expected and the SOL ions will be pushed toward the lower divertor, while SOL flow acceleration may be smaller in the outboard side since the flux surface is almost vertical and the trapped particle may have little radial excursion.

Figure 7. SOL flow pattern of negative triangularity snowflake single-null divertor plasma for a) ∇B away from X-point and b) toward X-point.

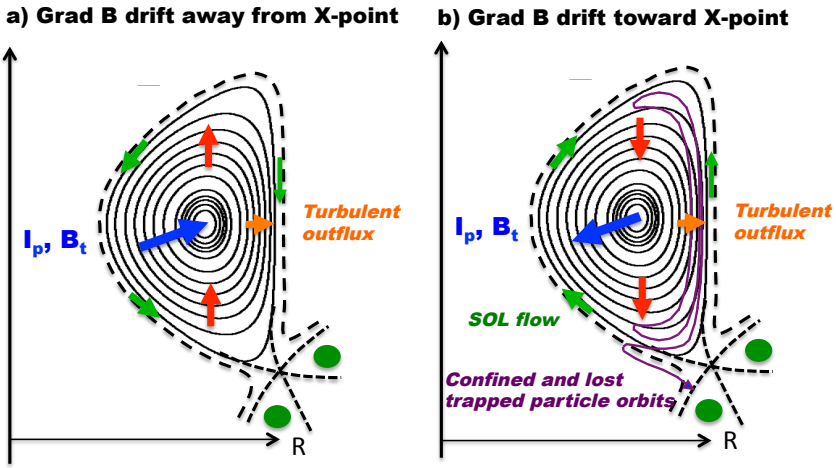

The structure of the SOL flow in the negative triangularity single null snowflake divertor may have a big difference for ∇B drift away from X-point and toward X-point as shown in Fig.7. In case of ∇B drift away from X-point, neoclassical acceleration of SOL flow directs to the X-point as shown in Fig.7

a), while it is opposite in case of ∇B toward X-point. Moreover, in case of ∇B toward X-point, the trapped ion orbit may has some loss orbit to make plasma negatively charged leading to the counter toroidal rotation without any external momentum sources.

Confinement Physics of Negative Triangularity:

The trapped electron mode (TEM) is one of important candidates of the turbulent transport in tokamak, for example by Kadomtsev [62] and recent experiments [35], [1] show TEM plays an important role in turbulent transport. The TEM growth is influenced by the mode resonance with the precession drift since perturbed distribution function $g_e \sim 1/(\omega - \omega_{De})$.

Figure 8. a) Trapped particle precession drift in toroidal direction from Kadomtsev[62]. b) Linear growth rate of TEM as a function of triangularity Δ from Rewoldt [58]. c) Normalized trapped particle toroidal drift as a function of bounce angle θ_b for $s = 0.25, q = 1$ from Connor [57].

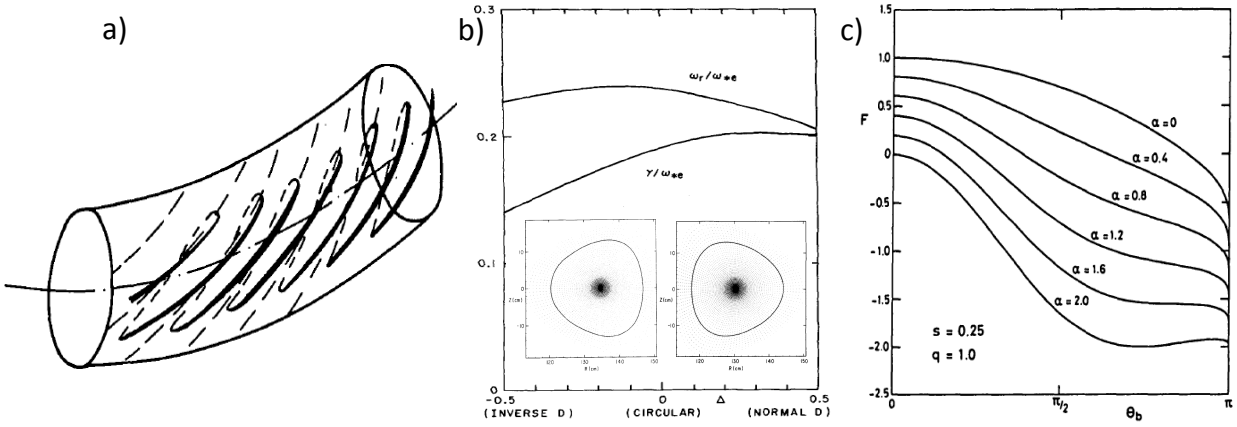

Finite beta drift reversal effect is first pointed out by Rosenbluth [61] and Connor [57] showed that large Shafranov shift can change the direction of the trapped particle precession drift and hence can affect the stability of TEM. Rewoldt [58] showed that the normalized linear growth rate of TEM, γ/ω_{*e} is reduced by shaping the plasma to have negative triangularity through the change in the precession drift resonance. Effect of negative shear on precession drift and TEM is shown by Kadomtsev [63] and has been discussed related to negative shear core improved confinement (ERS) in TFTR by Beer [50] and also discussed related to advanced tokamak scenario by Kessel [53].

TCV (Tokamak a configuration variable) s a flexible research tokamak of the Ecole polytechnique federale de Lausanne with the plasma major radius $R_p = 0.88m$ and the plasma current up to $1.2MA$ [49], [25].

A comparative study of positive and negative triangular plasmas in ohmically heated plasma gives an interesting parametric dependence by Moret [48] and extensive work in ECH heated L-mode plasma in the limiter configuration clarified quite interesting differences between positive and negative triangular plasmas by Camenen [31] as shown in Fig.8. The negative triangularity Tokamak has much better confinement even under the L-mode, for example, the negative triangularity L-mode requires half a

heating power to obtain the same plasma energy of standard D-shaped L-mode. In their TEM dominant experiments, χ_e strongly depends on the effective collisionality and also on the triangularity.

Figure 9. a) Negative and positive triangular plasmas in TCV. b) Electron thermal diffusivity χ_e as a function of effective collision time showing significant reduction of χ_e for negative triangularity plasma at same collision time by Camenen [31].

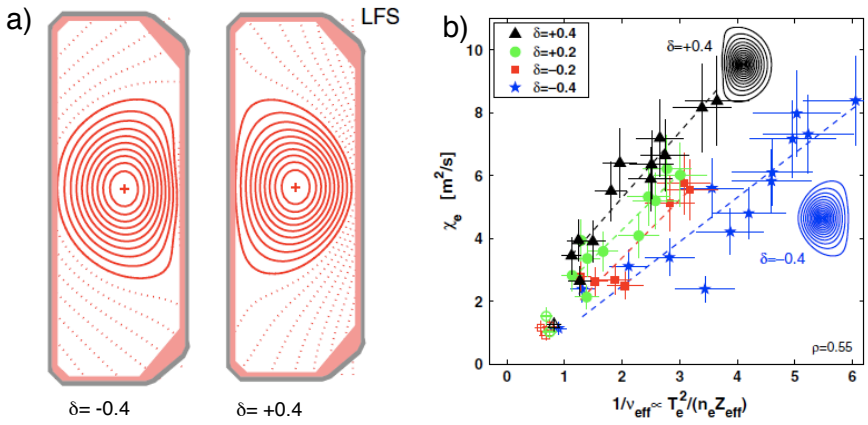

Camenen [31] also showed that the Shafranov shift is much bigger for the negative triangularity as shown in Fig.9 a). While the global linear eigenmode analysis of TEM gives almost same linear growth rate for positive and negative triangularity, the mixing length estimate of the electron thermal diffusivity $\chi_e \sim \gamma/k_\perp^2$ is appreciably smaller for the negative triangularity. Cause of this improved confinement may also be related to the linear eigenmode structure of the trapped electron mode (TEM) in the negative triangularity tokamak. While the mode is radially elongated in the standard D-shaped tokamak, the mode is tilted in the poloidal direction due to strong magnetic shear. This implies the reduced step size of the turbulent transport.

Figure 10. a) Shafranov shifts of negative and positive triangular plasmas. b) Global linear eigen mode structures of positive and negative triangularity plasma by Camenen [31].

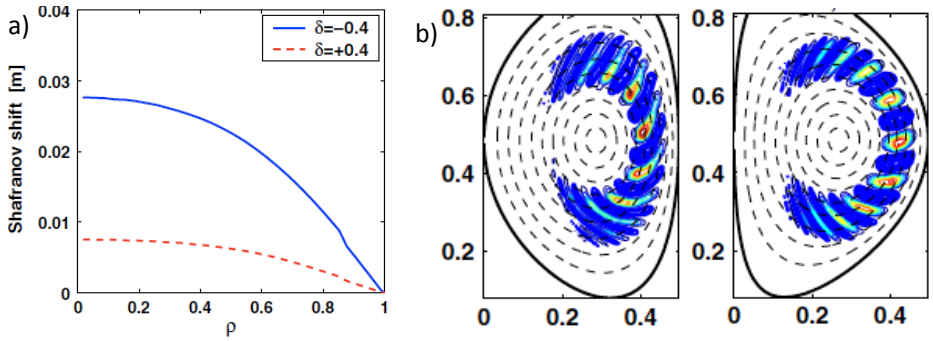

Sauter [5] developed a three region transport model with center, core and edge to find core to be stiff and edge to be non-stiff. He found center does not need improved confinement but core having same transport scaling $\chi_e \sim P^{0.7}$ and improved edge confinement expected from the non-linear gyrokinetic flux-tube simulation by Marinoni [20], which gives transport reduction may be limited to $r/a > 0.7$, can

explain better confinement of negative triangularity plasma. Global nonlinear gyrokinetic simulation may be important to clarify non-local effect such as ρ^* effect [16] may clarify key physics behind this improved confinement.

Another important question is the effect of the negative triangularity on the zonal flow. General expression of the residual zonal flow in toroidal plasma is given by,

$$\frac{\phi_k(t\rightarrow\infty)}{\phi_k(t=0)} = \frac{\epsilon^{pol}_{k,cl}}{\epsilon^{pol}_{k,cl}+\epsilon^{pol}_{k,nc}} \tag{3}$$

, where $\epsilon^{pol}_{k,cl}$ and $\epsilon^{pol}_{k,nc}$ are classical and neoclassical polarization, respectively. Parametric dependence of the residual zonal flow has been evaluated by Xiao [28] and residual zonal flow increases with elongation and also triangularity but they do not calculate residual zonal flow for the negative triangularity.

Trapped particles of Negative Triangularity:

The trapped particles produces a lot of physical processes in tokamak. Especially, the effect of negative triangularity to the bootstrap current is important from the steady state operation of the tokamak fusion reactor [8]. The parallel viscosity coefficients are proportional to the ratio of trapped particle fraction to the passing particle fraction($\mu^a_j \sim f_t/f_c$), where:

$$f_t = 1-\frac{3}{4}\langle B^2\rangle\int_0^{1/B_{max}}\frac{\lambda d\lambda}{\langle\sqrt{1-\lambda B}\rangle} \tag{4}$$

This trapped particle fraction depends primarily to the inverse aspect ratio $\epsilon = r/R$ but also has some dependence on triangularity as well. Sauter [47] found that f_t is more relevant parameter than ϵ for the electrical conductivity and also the bootstrap coefficients, which mainly comes from the fact that f_t is a function of the inverse aspect ratio ϵ and also the triangularity δ. The ratio f_t/f_c for negative and positive triangularity is shown in Fig11 a).

Figure 11. a) Trapped particle fraction as a function of ϵ for positive and negative δ. b) Bootstrap current coefficient L_{31} for positive and negative δ as a function of ε.

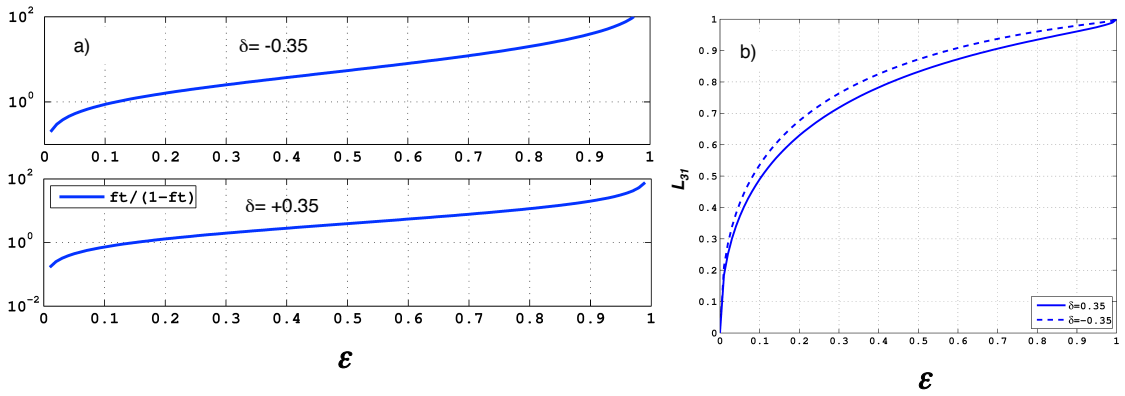

Thus, increased trapped particle fraction by the negative triangularity enhances the bootstrap coefficients as shown in Fig.11 b) such as L_{31} and L_{32} defined by:

$$\langle J_{bs}B\rangle \sim -Fn_e\frac{T_a}{|Z_a|}\left[L_{31}^a\frac{\partial lnp_a}{\partial\psi}+L_{32}\frac{\partial lnT_a}{\partial\psi}\right] \tag{5}$$

Sauter [5] gave a simple formula of the trapped particle fraction f_t including the dependence on the triangularity using $\epsilon_{eff}=0.67(1-1.4\delta|\delta|)\epsilon$ as follows,

$$f_t=1-\sqrt{\frac{1-\epsilon}{1+\epsilon}}\frac{1-\epsilon_{eff}}{1+2\sqrt{\epsilon_{eff}}} \tag{6}$$

EC Current Drive in Negative Triangularity:

Development of reactor relevant current drive in tokamak is crucial to realize continuous operation of tokamak. Among various non-inductive current drivers (Electron Cyclotron (EC) system, Neutral Beam (NB) system, Lower Hybrid (LH) system, Ion cyclotron (IC) system), EC system has robust coupling property, highest transmission power density and localized heating and current drive capability for better MHD and transport controls. However, O-mode EC current drive from the low field side has lower current drive efficiency and the problem of density limit. The fundamental X-mode EC current drive from high field side has higher current drive efficiency and density range can be much wider but is not possible for standard D-shaped tokamak due to tight space constraint in the inboard side. But high field side fundamental X-mode EC current drive may be possible since we have more space to locate EC launcher in high field side in the negative triangular plasma as seen in Fig.12.

Thus, an optimization of current drive efficiency and MHD control such as NTM stabilization by the fundamental X-mode injection from high field side is crucially important.

Figure 12. a) EC injection geometry for negative triangularity tokamak b) CMA diagram for fundamental X-mode injection. Low field side injection faces RH cutoff and can not reach fundamental EC resonance. RH cutoff gives density limit for the 2nd harmonic EC resonance. In case of high field launch shown by the red arrow allows easy access to the fundamental resonance.

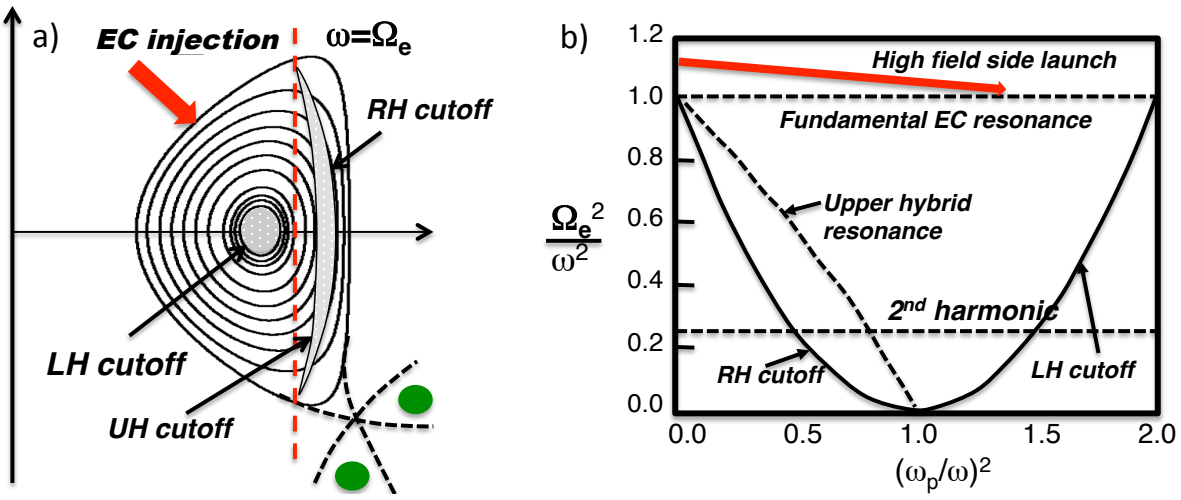

MHD Physics of Negative Triangularity:

Negative triangularity influences the behavior of sawtooth activity if there exist a region with $q < 1$. Martynov [36] investigated the variation of the sawtooth period for a wide range of triangularity showing a long sawtooth period for strongly negative triangularity, which may be related to the higher β_p^c against the internal kink stability as shown in Fig.13.

Figure 13. a) Sawtooth period dependence on δ_a, where $\delta_a = -0.6 \sim 0.3$ corresponds to $\delta_{q=1} = -0.1 \sim +0.055$. b) Contour plot of critical β_p for the internal kink mode in (κ, δ) plane. From Martynov [36]

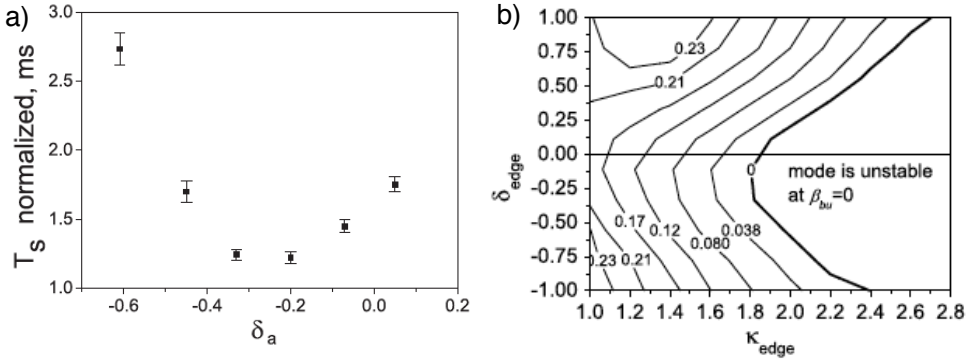

The edge MHD stability is most crucial item for the power handling in tokamak. Key design philosophy is to achieve "soft edge beta limit" instead of achieving highest possible beta for the steady state operation under the high bootstrap current fraction. This may lead to a fundamental change to the direction of the advanced tokamak research.

Figure 14. a) Stability diagram for Mercier and low n ideal MHD modes in LHD. b) Stability diagram with experimental data from LHD. From Watanabe [34]

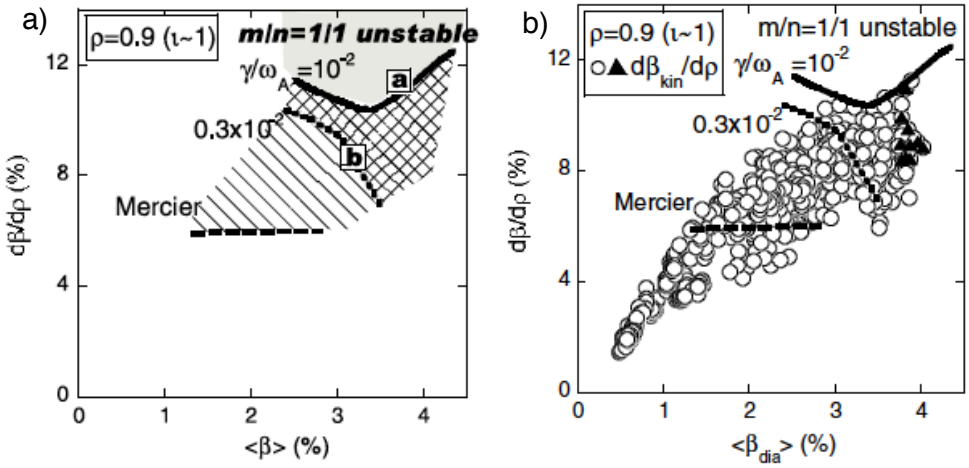

As we discussed in section 2.4, shape optimization tends to lead stabilization of high n modes such as ballooning modes through entering into the second stability regime. Then, the limiting edge MHD mode becomes low n peeling modes, which result in the severe ELM activity to damage the divertor plates.

If this view is correct, we have to find MHD design of tokamak edge to be limited by the high n ballooning modes or Mercier modes. The LHD experiments showed that plasma beta much above Mercier stability limit can be achieved as shown in Fig.14 [34]. This implies that we have to draw stability diagram for negative triangularity tokamak not limited by localized Mercier and ballooning limits but also the beta limit until low (m, n) ideal MHD limit. Actual beta limit should be determined experimentally or through the nonlinear MHD simulation.

Medvedev made a systematic works on the MHD stability of negative triangularity tokamak in TCV [26], [19], [13]. It is shown that Mercier mode can be unstable in the core even at $q > 1$ for the negative triangular plasma. As for the edge MHD stability of the negative triangularity tokamak, the 2nd stability access is closed and the most unstable mode becomes $n = \infty$ ballooning mode or Mercier mode in the pedestal region [26]. Since $n = \infty$ ballooning mode or Mercier mode may cause a soft beta limit or grassy ELM at the pedestal region, this closure of the 2nd stability regime may be favorable for the reduction of the ELM energy loss. Actually an increased ELM frequency in the H-mode is reported by Pochelon [11].

While negative triangularity plasma has some favorable MHD property to ELM, the beta limit is relatively low at $\beta_N \sim 2$ and also low n and high n mode stability limits are similarly low. Further optimization of the beta limit by combination of shaping and current profile is necessary.

Figure 15. a) Standard D-shaped tokamak in TCV and the stability diagram. b) Negative triangularity tokamak in TCV and its stability diagram [26]

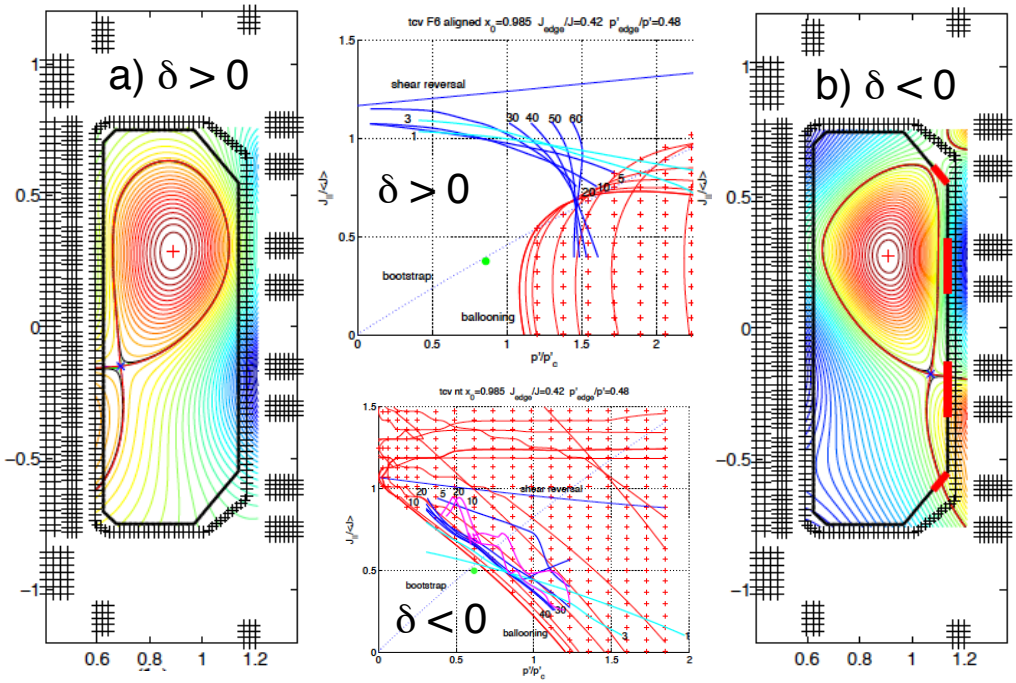

Technical Merits of Negative Triangularity:

There are some technical merits of the negative triangularity tokamak. We show obvious two merits.

1. Lower background magnetic field for internal poloidal field coils:

Other reactor studies such as Slim CS for implementing snowflake divertor show it is necessary to place the snowflake shaping coils inside the toroidal field coils. Even if we can have a divertor solution without snowflake, it is also true that the internal poloidal field coil system makes divertor configuration robust against plasma perturbations. Then there is significant merit for the negative triangularity tokamak since B_t is much weaker at the snowflake shaping coils, by which we may be able to use $NbTi$ superconductors for the shaping coils. At high background magnetic field, use of Nb_3Sn superconductor is necessary and the wind-and-react on machine has a lot of technical issues. In case of $NbTi$, it is quite robust against bending and much suited for internal poloidal field coils.

2. Larger pumping conductance from the divertor room:

In the standard D-shaped tokamak reactor design such as SSTR [56], the pumping duct design is the difficulty since thick 14MeV neutron shielding reduces the net pumping conductance from the inboard divertor room. In case of negative triangularity, the divertor room is in the outboard side, where we can have wider slot for horizontal and the vertical pumping duct. If we do not need snowflake, pumping duct design is much easier. Periodic replacement of the divertor cassette may be much easier as well.

Figure 16. a) Pumping duct design of SSTR [56]. b) Geometrical merit of pumping for negative triangularity tokamak.

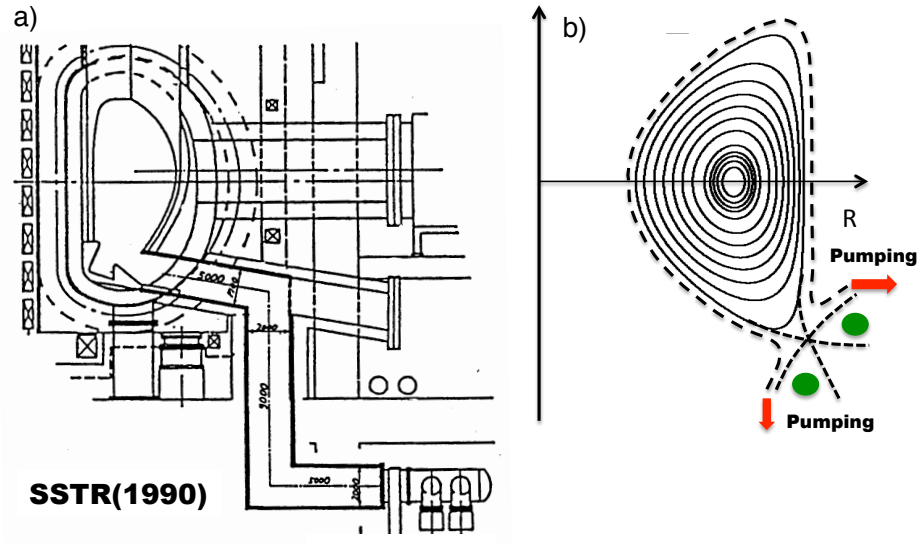

Acknowledgements

Main text.

References

1. W.L. Zhong et al., Phys. Rev. Lett. **111**, 265001(2013).
2. M. Kikuchi, T. Takizuka, Plenary Talk at US-EU TTF 2013 at Santa Rosa (USA) April 9-12, 2013, http://ttf2013.ucsd.edu/TTF_Meeting/Presentations.html.
3. T. Evans, Plenary Talk at US-EU TTF 2013 at Santa Rosa (USA) April 9-12, 2013, http://ttf2013.ucsd.edu/TTF_Meeting/Presentations.html.
4. O. Sauter, US-EU TTF 2013 at Santa Rosa (USA) April 9-12, 2013, http://ttf2013.ucsd.edu/TTF_-Meeting/Presentations.html.
5. O. Sauter, CRPP internal report 2013, No 06/2013 at http://infoscience.epfl.ch/record/187521?ln=fr.
6. N. Asakura et al., Nuclear Fusion **53**, 123013(2013).
7. N. Asakura et al., Trans. Fusion Science and Technology **63**, 70(2013).
8. M. Kikuchi, M. Azumi, Steady State Tokamak Research, Rev. Mod. Phys. **84**,1807(2012).
9. R.J. Goldston, Nuclear Fusion **52**, 013009(2012).
10. N. Aiba, N. Oyama, Nuclear Fusion **52**, 114002(2012).
11. A. Pochelon, et al., Plasma and Fusion Research **7**, 2502148(2012).
12. M. Kikuchi, *Frontier in Fusion Research - Physics and Fusion*, (Springer Verlag, 2011).
13. S. Medvedev, et al., Proc. 38th EPS on plasma physics, Strasbourg, France **35G**, P2.093(2011).
14. T. Eich et al., Phys. Rev. Lett. **107**, 215001(2011).
15. T. Takizuka, et al., Contrib. Plasma Phys. **50**, 267(2010).
16. B.F. McMillan, et al., Phys. Rev. Lett. **105**, 155001(2010).
17. D.G. Whyte et al., Nuclear Fusion **50**, 105005(2010).
18. H. Frerichs et al., Nuclear Fusion **50**, 034004(2010).
19. S. Medvedev, et al., Proc. 37th EPS on plasma physics, Dublin, Ireland **34A**, P4.145(2010).
20. A. Martinoni et al., Plasma Phys. Contr. Fusion **51**, 055016(2009).
21. T. Takizuka et al., Nuclear Fusion **49**, 075038(2009).
22. N. Hayashi et al., Nuclear Fusion **49**, 095015(2009).
23. A. Wingen et al., Nuclear Fusion **49**, 055027(2009).
24. D.D. Ryutov et al., Phys. Plasmas **15**, 092501(2008).
25. A. Fasoli et al., Nuclear Fusion **48**, 034001(2008).
26. S. Medvedev, et al., Proc. 35th EPS on plasma physics, Hersonissos, ECA **32D**, P-1.072 (2008).
27. A. Loarte et al., Nuclear Fusion **47**, S203(2007).
28. Y. Xiao, et al., Phys. Plasma **14**, 055910(2007).
29. D.D. Ryutov, Phys. Plasma **14**, 064502(2007).
30. A.V. Chankin et al., Nuclear Fusion **47**, 762(2007).
31. Y. Camenen et al., Nuclear Fusion **47**, 510(2007).
32. T.E. Evans, et al., Nuclear Fusion **45**, 595(2005).
33. H. Kishimoto, et al., Nuclear Fusion **45**, 986(2005).
34. K.Y. Watanabe, et al., Nuclear Fusion **45**, 1247(2005).
35. F. Ryter et al., Phys. Rev. Lett. **95**, 085001(2005).
36. A. Martynov, J.P. Graves, O. Sauter, Plasma Physics and Controlled Fusion **47**, 1743(2005).

37. P.T. Lang, et al., Nuclear Fusion **44**, 665(2004).
38. A. Loarte, et al., Plasma Physics and Controlled Fusion **45**, 1549(2003).
39. R.J. Hastie, et al., Phys. Plasmas **10**, 4405(2003).
40. D.A. Sossessian, et al., Plasma Physics and Controlled Fusion **44**, 423(2002).
41. M. Keilhacker, et al., Nuclear Fusion **41**, 1925(2001).
42. G. Federici, et al., Nuclear Fusion **41**, 1967(2001).
43. K. Burrell, et al., Phys. Plasmas **8**, 2153(2001).
44. J. Stober, et al., Nuclear Fusion **41**, 1123(2001).
45. Y. Kamada et al., Plasma Physics and Controlled Fusion **42A**, A247(2000).
46. H. Reimerdes et al., Plasma Physics and Controlled Fusion **42**, 629(2000).
47. O. Sauter, et al., Phys. Plasmas **6**, 2834(1999).
48. J.M. Moret et al., Phys. Rev. Lett. **79**, 2057(1997).
49. J.B. Lister, et al., Fusion Technology **32**, 321(1997).
50. M.A. Beer, et al., Phys. Plasmas **4**, 1792(1997).
51. H. Zohm et al., Plasma Physics and Controlled Fusion **38**, 105(1996).
52. C.M. Roach, et al., Plasma Physics and Controlled Fusion **37**, 679(1995).
53. C. Kessel et al., Phys. Rev. Lett. **72**, 1212(1994).
54. M. Kikuchi, Plasma Physics and Controlled Fusion **35**, B39(1993).
55. N. Ueda, M. Tanaka, M. Kikuchi, Y. Seki, Nuclear Fusion **32**, 253(1992).
56. M. Kikuchi, R. Conn, F. Najmabadi, Y. Seki, Fusion Engineering and Design **16**, 253(1991).
57. J.W. Connor, et al., Nuclear Fusion **23**, 1702(1983).
58. G. Rewoldt, et al., Phys. Fluids **25**, 480(1982).
59. W. Tang, J.W. Connor, R.J. Hastie, Nuclear Fusion **20**, 1439(1980).
60. M. Azumi, et al., Proc. 8th Int. Conf. Plasma Phys. Contr. Nucl. Fus. Res.,1980. **1**, 293(1981).
61. M.N. Rosenbluth, , et al., Phys. Fluids **25**, 480(1982).
62. B.B. Kadomtsev, O.P. Pogutse, Nuclear Fusion **11**, 67(1971).
63. B.B. Kadomtsev, O.P. Pogutse, *Reviews of Plasma Physics Vol 5*, (Consultants Bureau, NY, 1970): Also Sov. Phys. JETP **24**, 1172(1967).